On Ocean Dynamics in Midlatitude Climate

WILLIAM K. DEWAR

Department of Oceanographyo and School of Computational Science and Information Technology, The Florida State University, Tallahassee, Florida

(Manuscript received 21 September 2000, in final form 9 July 2001)

ABSTRACT

Several recent models of midlatitude climate have speculated on the role of the North Atlantic Ocean in modulating the North Atlantic oscillation (NAO). Here this role is examined by means of numerical experimentation with a quasigeostrophic ocean model underneath a highly idealized atmosphere. It is argued that the dominant midlatitude oceanic influence is due to the so-called inertial recirculations, rather than linear baroclinic waves, as have previously been studied.

In these experiments, the forced response of the inertial recirculations dominates the leading-order ocean spatial mode, but that mode is energized by oceanic intrinsic variability. The oceanic signals are amplified relative to those predicted by wave models. The primary oceanic role of the coupling is to damp sea surface temperature (SST) at longer timescales, and the interdecadal atmospheric variability is placed under the control of the ocean. The SST damping reflects competition between intrinsically driven intergyre heat flux and an opposing feedback-driven advective heat flux. Spectral SST extrema can result near the transition point where the feedback heat flux approaches equilibrium, although these are secondary phenomena.

The picture of midlatitude climate variability painted here has qualitative similarities to that obtained from the linear waves models, but differs fundamentally from them both dynamically and philosophically. Most important, ocean variability is a dominant, rather than passive, partner in all aspects of the coupled system.

1. Introduction

In recent years, a recognition of the North Atlantic oscillation (NAO) as a primary mode of midlatitude climate variability has developed (Hurrell 1995) and the dynamical role of the ocean in the NAO has become of interest. This role has been explored in recent process dynamical studies, although the ocean has largely been limited to linear dynamics. The hypothesis behind the present work is that, if anything, it is nonlinear ocean dynamics that are relevant to midlatitude climate variability. The objective of this paper is to test this hypothesis by examining simple coupled models employing an ocean model where linear and nonlinear processes can compete.

a. Background

Oceanic SST variability in the North Atlantic is dominated by the so-called North Atlantic tripole (see Fig. 1), the northern two lobes of which are potentially connected to the NAO. Recently, indirect evidence for coupling between the North Atlantic Ocean and the NAO has been reported in the atmospheric general circulation model (GCM) studies by Rodwell et al. (1999) and Mehta et al. (2000), who noticed an overall improvement in their computed NAO model index when forced by observed North Atlantic SSTs. Although the interpretation of these results has been the subject of recent debate (Bretherton and Battisti 2000; Czaja and Marshall 2000), interest in the role of the midlatitude North Atlantic in the coupled climate has intensified.

Ocean–atmosphere coupling as an effect on climate variability is a classic problem. Bjerknes (1964) was the first to argue a climate role for the oceans, suggesting that sea surface temperature (SST) anomalies could be important in steering the atmospheric midlatitude storm track. A recent climate study supporting a comparable oceanic role was the coupled GCM study by Latif and Barnett (1994). They focussed on the Pacific and argued midlatitude planetary waves drove near-surface heat anomalies that, in turn, influenced wind stress. Other coupled GCM studies, however, have found less evidence of a midlatitude oceanic role (see Saravanan 1998).

Process models have also examined various aspects of the coupled climate system. A common theme of these is a dynamically linear ocean forced by and feeding back on simple atmospheres. Saravanan and McWilliams (1997) suggest stochastic NAO forcing in

Corresponding author address: William K. Dewar, Dept. of Oceanography and School of Computational Science and Information Technology, The Florida State University, Tallahassee, FL 32306.
E-mail: dewar@ocean.fsu.edu

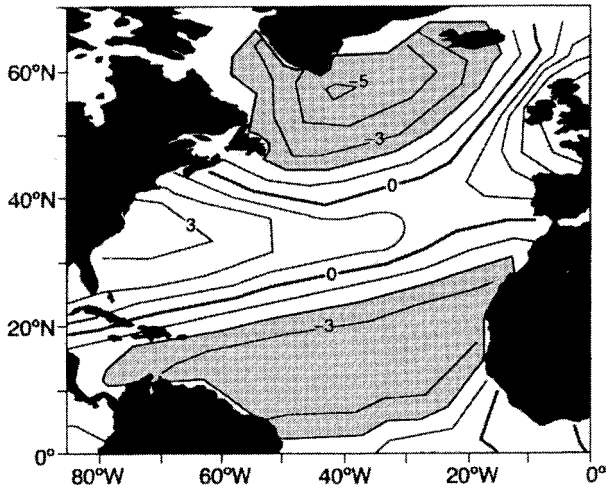

FIG. 1. The North Atlantic tripole in SST. This is the dominant pattern that regresses on the NAO index (in units of 0.1 kelvin).

the presence of an oceanic meridional overturning cell can result in a preferred ocean timescale for atmospheric variability. Münnich et al. (1998), argue for the importance of propagating baroclinic waves in the Pacific in a manner similar to that described by Latif and Barnett (1994). Jin (1997) and Neelin and Weng (1999) proposed models consisting of a wind stress field whose amplitude depended on the oceanic SST gradient. The models were forced by temporally stochastic, but spatially organized, atmospheric fields. Recently, Marshall et al. (2001, hereinafter MJG), generalized these models as well as several others in which the ocean is far more passive (Frankignoul and Hasselman 1977; Frankignoul et al. 1997).

An interdecadal peak in SST and atmospheric spectra appear in the latter models because of the wave-driven adjustment of the ocean circulation. Interest in those models has grown because recent analyses of ocean SST indices show an interdecadal spectral peak, and components of the NAO time series have suggested a similar atmospheric low-frequency response (Czaja and Marshall 2000). However, while Czaja and Marshall (2000) argue their peaks are statistically significant, GCM evidence for the postulated midlatitude coupling is weak. A different view was taken by Cessi (2000, manuscript submitted to *J. Climate*; see also Gallego and Cessi 2000; Primeau and Cessi 2001) who identified nonlinear processes in the coupled system as a source of variability.

b. This paper

In summary, observations show structure in midlatitude ocean–atmosphere spectra and recent simple models offer possible dynamical explanations for them. We continue the study of process coupled climate models in the present paper, although we extend them beyond the limits they have realized to date. Of the many assumptions in the above models, we primarily address the adequacy of linear ocean dynamics. Our hypothesis is that the dominant ocean input into midlatitude variability is the product of nonlinear ocean dynamics. The importance of nonlinearity is suggested by 20 years' worth of ocean-only model studies, arguing that the northwestern corner of the subtropical gyre is highly inertial in parameter ranges characteristic of the open ocean. Such regions are potentially critical to the coupled climate system in that they compose the locations of maximum midlatitude ocean–atmosphere buoyancy exchange and are central to heat flux between subtropical and subpolar ocean gyres. In view of this, it is plausible that the regional dynamics of the recirculations have a role to play in the coupled climate system. In fact, experimentation with simple ocean models in nonlinear regimes (not shown here) argue linear waves are largely masked at the intergyre boundary by the intrinsic variability of the inertial gyres. This suggests at the least that, if the oceans participate in midlatitude coupled climate dynamics, those process models emphasizing the role of propagative oceanic waves in intergyre heat transport will be subject to modification by inertial dynamics. Another possibility is that it is oceanic variability driven by intrinsic ocean dynamics that feeds back on the atmosphere.

Accordingly, the results of this study lean heavily toward the latter case. We show that intrinsic variability, as an effect on SST through intergyre transport, is a very red process. The intergyre flux involves a large-scale oceanic response that manifests itself primarily in the inertial recirculations. In coupled models, SST anomalies feed back on the wind stress field to drive an intergyre heat flux in opposition to that of the intrinsic variability; at leading order these two fluxes balance. Thus, the most important oceanic effect of coupling is that SST variability is suppressed and the spectra roll off to white from red. Secondarily, SST spectral peaks can result. In these experiments, the atmospheric variables are completely controlled by the ocean. Further, model spectral signatures in atmospheric variables and SST are qualitatively similar to those recently discussed by Czaja and Marshall (2000). The delayed oscillator models forwarded elsewhere share a qualitative similarity with the present model in that equilibration, here of the inertial recirculations, is fundamentally involved. On the other hand, dynamically and philosophically, the models are quite distinct and their implications for the coupled midlatitude climate greatly differ.

We argue these points by examining a fully nonlinear quasigeostrophic (QG) ocean model forced at the surface by a mean wind combined with an idealized stochastic NAO wind stress and a stress feedback proportional to the subpolar–subtropical SST gradient. Oceanic SST is computed using a highly simplified mixed layer, where advection is provided by the QG model. This calculation follows closely those of Jin (1997), Neelin and Weng (1999), and particularly MJG, aside from the

use of full QG dynamics. As such, it represents the simplest possible test of ocean nonlinearity in the coupled climate system.

The model is developed in the next section, where its connections to previous studies are emphasized. Section 3 describes the analysis of the model solutions and section 4 concludes the paper with discussion and thoughts on future work.

2. Model development

a. Atmospheric model

Following previous studies, wind stress $[\hat{\tau}^{(x)}, \hat{\tau}^{(y)}]$, is calculated according to

$$\hat{\tau}^{(x)}(x, y, t) = \rho_o[\hat{\kappa}\hat{N}(x, y, t) - \hat{f}T'_y/2 + \tau_o(x, y)]$$
$$\hat{\tau}^{(y)} = 0, \tag{1}$$

where τ_o is a mean wind stress field, ρ_o is an average water density, $\hat{N}$ is a temporally stochastic input whose spatial distribution is set by the NAO structure, and $\hat{f}T'_y$ is the feedback on wind stress due to anomalies in the sea surface temperature gradient. The quantity $\hat{\kappa}$ scales the nondimensional $\hat{N}$ into the units of wind stress.

Consistent with the simplicity of our approach, a rectangular ocean basin is assumed. The mean stress generates a mean Ekman pumping field of

$$w_{eo} = \mu_o \sin(\pi y/L) \tag{2}$$

for $-L < y < L$, where L is the half-basin meridional length. This generates a classic subtropical–subpolar gyre pair and has received extensive study. We chose values for μ_o from 2.5×10^{-6} to 5×10^{-6} m s^{-1}, which are comparable to those inferred for the open ocean. The variable part of the stress generates a time-dependent Ekman pumping w'_e according to

$$w'_e = \begin{cases} a(t)\cos(\pi y/L_N); & |y| < L_N/2 \\ 0; & |y| > L_N/2, \end{cases} \tag{3}$$

where $L_N/2$ denotes the meridional scale of the variability. We have used a basin of 2000-km meridional extent, and confined the stochastic input to 500 km on either side of $y = 0$ (see Fig. 2). Thus our model NAO structure is more latitudinally restricted than the ocean circulation gyres, roughly consistent with the oceanographic setting. The spatial distribution of these anomalies is assumed fixed, in keeping with Jin (1997) and others.

The stochastic NAO stress and SST anomalies are similar in spatial structure. We therefore isolate the temporal part of these inputs as

$$a(t) = -(\kappa N - f\Delta T/2), \tag{4}$$

where the quantity N is dimensionless and marks the time-dependent part of the atmospheric wind stress anomaly $\hat{N}$, and $\Delta T = T_n - T_s$ is the net temperature difference between the northern and southern SST lobes (denoted T_n and T_s, respectively). The variables $f = \hat{f}/(f_o\Lambda^2)$ and $\kappa = \hat{\kappa}/(f_o\Lambda)$, where Λ is a length scale representative of the anomalous stress field. Equation (4) is essentially the atmospheric model discussed in Jin (1997), Neelin and Weng (1999), and MJG.

Atmospheric spectra are largely white for periods longer than about one month (Frankignoul et al. 1997); therefore, N is modeled as a random, normally distributed variable of unit variance, filtered to remove energy at frequencies higher than 1 cycle per 2 weeks. Positive ΔT is associated with warm northern and cold southern temperatures, and thus a weakening of the SST change between the subpolar and subtropical gyres. The sign of the feedback coefficient f is positive, indicating for this case that the wind stress weakens and an upwelling anomaly is induced [see (4)]. Typical wind stress curls for the North Atlantic are on the order of 10×10^{-8} N m^{-3}, while those correlated with the NAO are smaller than, but comparable to, this value (MJG). In our experiments, we have used $\kappa = (0.5 - 1)\mu_o$. MJG and Czaja and Marshall (2000) examine test cases for which the feedback parameter f, given North Atlantic temperature anomalies of 1 K, generates pumping variability on the order of 10% of the mean. In our experiments, we have used $f = (0.1 - 10.2)\mu_o/(\text{K})$.

b. Ocean model

The SST equation is

$$T_t + \nabla\cdot(\mathbf{u}T) = -\nabla\cdot\mathbf{F}, \tag{5}$$

where T denotes SST, $\mathbf{u}$ velocity, and $\mathbf{F}$ is diffusive heat flux. All variables are written as the sum of mean and perturbation quantities, for example, $T = T_o + T'$. Integrating (5) over the southern half volume of fluid enclosed by the mean circulation yields

$$\frac{\partial}{\partial t}\iiint T'\, dV = -\iint \mathbf{u}T_o\cdot\mathbf{n}\, dS - \iint \mathbf{F}\cdot\mathbf{n}\, dS, \tag{6}$$

where $\mathbf{n}$ is an outward-pointing unit vector on the bounding surface S of the integration volume. There is no contribution by mean advection due to the choice of integration volume, and perturbation temperature flux is ignored in (6) to retain similarity with the above process models. Fluxes on all solid boundaries vanish and assuming diapycnal heat flux is largely confined to near-surface isopycnals for the timescales of interest, we can restrict the volume and surface integrals in (6) to that range of isopycnals. Dividing by fluid volume V yields

$$\frac{\partial}{\partial t}T_s = -\frac{\iint v'T_o\, dS}{V} - \lambda T_s + \hat{\alpha}N, \tag{7}$$

where the volume-averaged temperature perturbation is denoted T_s and the perturbation atmospheric heat flux has been written as a relaxation of the perturbation temperature and a contribution due to anomalous atmo-

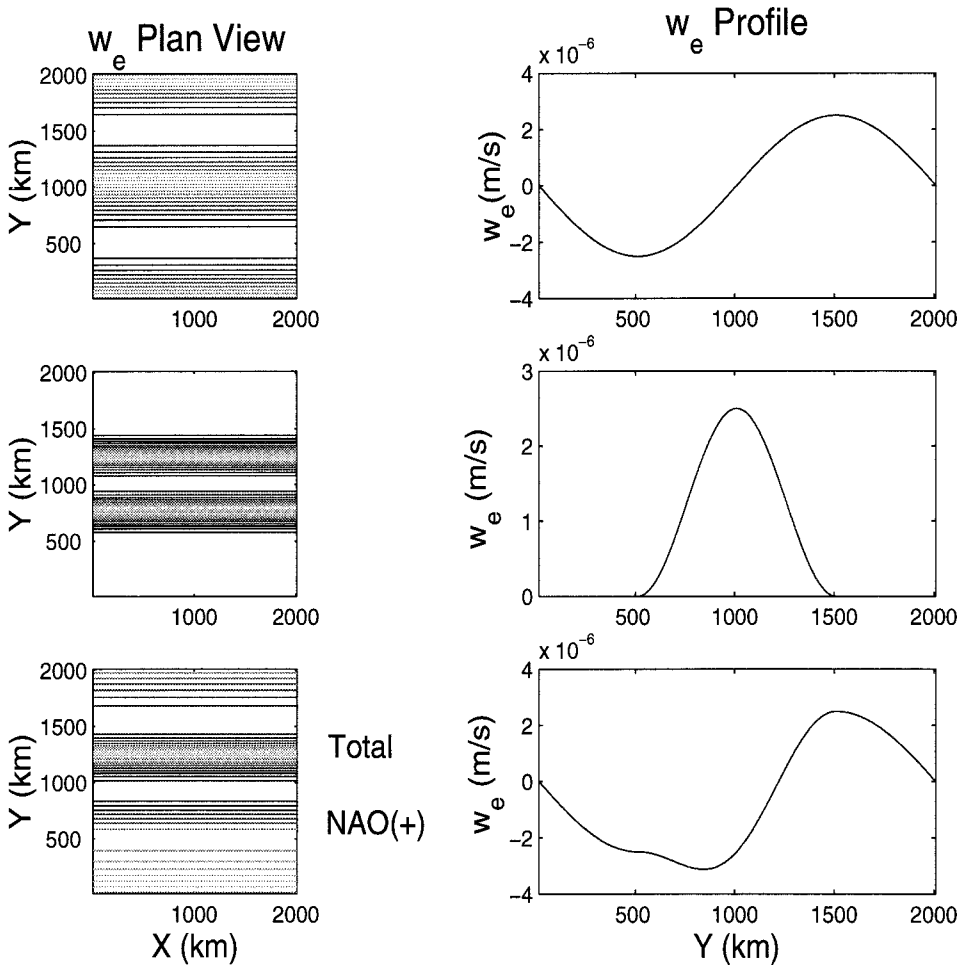

FIG. 2. Model Ekman pumping. The upper-left panel shows the mean, classic double gyre forcing. The upper-right panel is a cross section from north to south through the mean field. The middle row shows the perturbation pumping field associated with the NAO. The lower row shows the pumping associated with a period of maximum positive NAO anomaly.

spheric heat flux forcing. We will routinely identify the volume V in (7) with a volume of 500 km $\times$ 2000 km $\times$ 200 m, corresponding to the zonal size of our model basin, the meridional extent of the dominant variability and an assumed 200-m typical mixed layer depth. The horizontal area of V is comparable to that of the westernmost center of SST activity in the recurrence maps of Czaja and Marshall (2001).

A similar procedure can be followed for the northern gyre, resulting in an equation for the averaged northern temperature anomaly T_n. The difference of these two anomalies ΔT enters into (4). Analyzing these equations demonstrates the sum of the temperature anomalies quickly approaches zero, yielding $T_s = -T_n$. We thus consider only (7) in the following. In general, when SST is mentioned hereinafter, the variable T_s is meant.

In our standard experiments, $\lambda \sim (\text{yr})^{-1}$, representing roughly a relaxation coefficient of 25 W m^{-2} K^{-1} acting on a mixed layer of 200-m depth. This is similar to that used in MJG. The stochastic input uses the same random temporal variable N as the wind stress because anomalous atmospheric heat fluxes and stresses are correlated. In our experiments, $\hat{\alpha} = (1\text{–}4)\ \text{K}\lambda \sim (1 - 4)\ \text{K yr}^{-1}$. Setting $\hat{\alpha} \approx 1\ \text{K}\lambda$ is largely consistent with MJG and Czaja and Marshall (2000), the latter using $\hat{\alpha} = 1.8\ \text{K}\lambda$.[1]

1) A REVIEW OF LINEAR MODELS

The intergyre heat exchange is the product of the mean state temperature and perturbation velocity on the mean gyre boundary. The MJG model and others like it compute velocity using linear waves, that is,

[1] We often vary $\hat{\alpha}$ and κ independently during numerical parameter variations. A reviewer has rightly pointed out that these two quantities are not independent, with atmospheric heat flux strongly coupled to wind stress. Our results are largely insensitive to these parameters, so independently manipulating heat and momentum fluxes will not influence model outcomes.

$$h_t - ch_x = -w_e', \tag{8}$$

where $w_e' = \nabla \times (\boldsymbol{\tau}'/f)$ is the variable Ekman pumping along the gyre boundary, c is the long planetary wave speed, and h is the thermocline depth. Straightforward manipulation yields (see MJG for details):

$$\upsilon_w = \frac{-g' w_e^o h_m}{f_o} \int_{t-L/c}^{t} a(t')\, dt'$$

$$= \frac{g' w_e^o h_m}{f_o} \int_{t-L/c}^{t} (\kappa N + fT_s)\, dt', \tag{9}$$

where υ_w is western boundary current transport, g' is the upper-layer reduced gravity, f_o is the Coriolis parameter, and L is the zonal basin extent. MJG further assume the cross-gyre boundary heat transport is dominated by western boundary layer transport of water warmer than that in the interior by an amount δT. Thus, substituting (9) in (7) yields

$$T_{st} = -\frac{\upsilon_w \delta T}{V} - \lambda T_s + \hat{\alpha} N. \tag{10}$$

MJG approximated the system as a delayed oscillator {i.e., (9) was written as $\upsilon_w = g' w_e^o a[t - L/(2c)]/f_o$} for physical clarity, although the analytical solution can be found. In the limit of $\omega \to 0$, the analytically expected temperature spectrum is

$$E_T = \frac{[\hat{\alpha} - \delta T g' w_e^o \kappa/(L_N c f_o)]^2 E_n}{[\lambda + \delta T g' w_e^o f/(L_N f_o c)]^2}, \tag{11}$$

demonstrating that coupling ($f \neq 0$) reduces temperature variance at low frequency. The full SST spectral structure predicted by the above linear models appears in Fig. 3, where coupled and uncoupled spectra are shown. The parameter settings for these curves are from the standard set (to be defined later), except as indicated in Fig. 3. SST spectral peaks can occur in uncoupled cases, although for oceanic settings coupling is generally needed to get a peak. In all cases, spectral peaks are always enhanced by coupling, and comparable peaks in the atmospheric variables of course are absent in the uncoupled case. An important point for later reference is that both uncoupled and coupled spectra roll off to white at low frequencies.

The numerator in (11) is related to the heat transport efficiency of the circulation. The quantity $\hat{\alpha}$ marks the net anomalous heat input into the gyre by the atmospheric stochastic heat flux. For $\hat{\alpha} = 1$–$4\ \mathrm{K}\lambda$ (the values studied here), the net stochastic atmospheric heat forcing is roughly

$$\hat{\alpha}\rho_o C_p V = \left[\frac{(3 - 12) \times 10^{-8}\ \mathrm{K}}{\mathrm{s}}\right]\left(\frac{1000\ \mathrm{kg}}{\mathrm{m}^3}\right)\left(\frac{4000\ \mathrm{J}}{\mathrm{kg\ K}}\right)$$

$$\times (2000\ \mathrm{km} \times 500\ \mathrm{km} \times 200\ \mathrm{m})$$

$$= (0.02 - 0.08)\mathrm{PW}$$

as compared with the observed net atmospheric heat flux value of 0.08 PW (MJG). The remainder of the numerator measures the oceanic intergyre heat flux. The Ekman pumpings used here generate transports S of

$$S = \frac{g' \kappa w_e^o L h_m}{(f_o c)}$$

$$= \frac{\left(\frac{0.03\ \mathrm{m}}{\mathrm{s}^2}\right)(0.5)\left(\frac{2.5 \times 10^{-6}\ \mathrm{m}}{\mathrm{s}}\right)(2000\ \mathrm{km})(200\ \mathrm{m})}{\left(\frac{10^{-4}}{\mathrm{s}}\right)\left(\frac{0.04\ \mathrm{m}}{\mathrm{s}}\right)}$$

$$= 3.8\ \mathrm{Sv},$$

3.8 Sv in a 200-m-deep mixed layer. Assuming a 6-K temperature difference along the intergyre boundary, this transport can more than balance the observed net atmospheric heat flux. Thus our standard parameter settings make the circulation a very efficient transporter of heat. This intent is in keeping with MJG, although their circulation was not as efficient as that of our standard parameters.

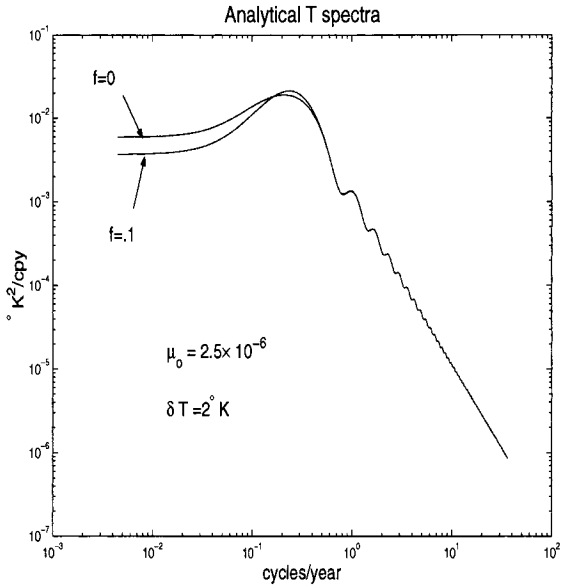

FIG. 3. Analytical spectra from both uncoupled and coupled cases. Coupling always enhances peaks, as evidenced by the $f = 0.1$ line.

2) A NONLINEAR MODEL

We substitute a three-layer quasigeostrophic model for (8). The QG dynamics support nonlinear ocean features well, and are simple enough to permit extensive investigation. The equations governing the three-layer model are

$$q_{1t} + J(\psi_1, q_1) = \frac{f_o}{H_1} w_e + K\nabla^4 \psi_1;$$

$$q_1 = \nabla^2 \psi_1 - \frac{f_o}{H_1} h_1 + \beta y$$

$$q_{2t} + J(\psi_2, q_2) = K\nabla^4\psi_2;$$

$$q_2 = \nabla^2\psi_2 - \frac{f_o}{H_2}(h_2 - h_1) + \beta y$$

$$q_{3t} + J(\psi_3, q_3) = K\nabla^4\psi_3 - r\nabla^2\psi_3;$$

$$q_3 = \nabla^2\psi_3 + \frac{f_o}{H_3}h_2 + \beta y \qquad (12)$$

expressing the evolution of potential vorticity (q_i) in layer i. The quantities ψ_i represent layer streamfunctions, f_o is the Coriolis parameter, H_i is the layer mean state thicknesses, h_i are interface perturbations [given by $h_i = f_o(\psi_i - \psi_{i+1})/g_i$ with g_i the interfacial reduced gravities], J is the usual Jacobian operator, β is the Coriolis gradient, K are viscosities, and r is related to the bottom drag. Subscripted t denotes a time derivative. The numerical implementation used here was described originally in Holland (1978). Spatial resolutions of 10 km were used and the deformation radii were $R_d = 45.8$ and 19.5 km for the first and second modes, respectively. Layer thicknesses were set to 500, 500, and 4000 m for the upper, middle, and lower layers. No-slip boundary conditions were applied and $K = 300\ \mathrm{m}^{-2}\ \mathrm{s}$.[2] This puts us in a high Reynolds number category (Berloff and McWilliams 1999). Bottom drag decay timescales (r^{-1}) of 200–1000 days were employed.

The model upper-layer pressure was used to diagnose the intergyre velocity at each grid point along $y = 0$. Mixed layer velocity in general contains an ageostrophic Ekman contribution. However, in our case, perturbation wind stress vanishes at $y = 0$, implying no Ekman transport contribution to (10). Intergyre heat flux was computed using an assumed mean state temperature profile of $T_o = \delta T(L - x)/L$, where x is zonal location. The model was routinely spun up for 5 yr from a state of rest. The runs were continued for an additional 200 yr archiving the various contributions to (10), at intervals of 5 days, as well as the model upper-layer pressure, subsampled at 30 km, at intervals of 30 days.

c. Standard parameters

We define our standard parameter set as $\hat{\alpha} = 3 \times 10^{-8}\ \mathrm{K\ s^{-1}}$, $\lambda = 3 \times 10^{-8}\ \mathrm{s^{-1}}$, $r^{-1} = 200$ days, $\delta T = 6$ K, and $\mu_o = 2.5 \times 10^{-6}\ \mathrm{m\ s^{-1}}$. Our standard coupled set consists of these plus $\kappa = \mu_o$ and $f = 0.2\ \mu_o\ \mathrm{K^{-1}}$. We discuss also standard uncoupled runs, meaning the standard coupled set with $f = 0$. The standard uncoupled runs can be either with or without noise, meaning $\kappa = \mu_o$ or $\kappa = 0$, respectively. Variations from the standard sets will be noted. Spectra frequently appear. These were computed using the multitapering MATLAB function PMTM with the time bandwidth parameter NW set to four. Standard 95% confidence intervals for these spectra were computed using the MATLAB χ^2 approach (Mathworks 2000).

[2] For our resolutions, the circulations computed using our version of the Holland model resemble the mixed boundary condition solutions found by Haidvogel et al. (1992) when slip boundary conditions dominate.

3. Numerical results and analysis

a. Mean states

In Fig. 4 we show examples of representative mean upper-layer streamfunctions computed over the last 200 years of experiments with feedback. The experiment on the left used the standard coupled parameters; the one on the right varied by $\mu_o = 5 \times 10^{-6}\ \mathrm{m\ s^{-1}}$ and $r^{-1} = 1000$ days. The gyre structures are essentially symmetric about the center latitude in both cases, consistent with our assumption about where to compute the intergyre heat exchange. The upper-layer transport in Sv appears in the upper panels and the total transport in the lower panels. The main difference between the left and right columns is in the strength of the flows. The left-hand upper panel has a net transport of about 28 Sv compared to the right-hand panel maximum of 48 Sv. The maximum upper-layer speed is 0.65 m s^{-1} on the left, and 0.95 m s^{-1} on the right. Lower-layer mean flows are dominated by the inertial recirculations, which appear in Fig. 4 in the latitudinally confined recirculations centered on the separated western boundary current. The total transport ranges from 40 to 125 Sv.

These circulations are the extreme cases of the circulations considered in this study. The left-hand column is relatively weak in total transport compared to the North Atlantic, although the mean upper-layer speeds, as averages over the upper 500 m, are reasonable. The right-hand column has a more realistic total transport. This plot suggests the parameter regime studied here is relevant to the oceanic case. In what follows, we will often show results from the standard coupled (weaker mean flow) case; but, the important characteristics of the experiments all occur in the more nonlinear cases.

b. What is the effect of coupling?

Of primary interest here is model SST. Coupling in the linear models damps temperature variance at lower frequencies. We have examined coupling in the present nonlinear model by conducting a set of experiments where the set members differ only in their exposure to the atmosphere. The members are the standard coupled parameter set and the standard uncoupled set, both with and without noise. Variations about the standard parameter set were also studied.

The temperature spectra from the standard experiments are compared in Fig. 5. Note, the low-frequency end of the coupled model is suppressed relative to both uncoupled models. This behavior was insensitive to variations of the parameters μ_o, f, and $\hat{\alpha}$ (results not shown here). The two uncoupled runs in this plot are differ-

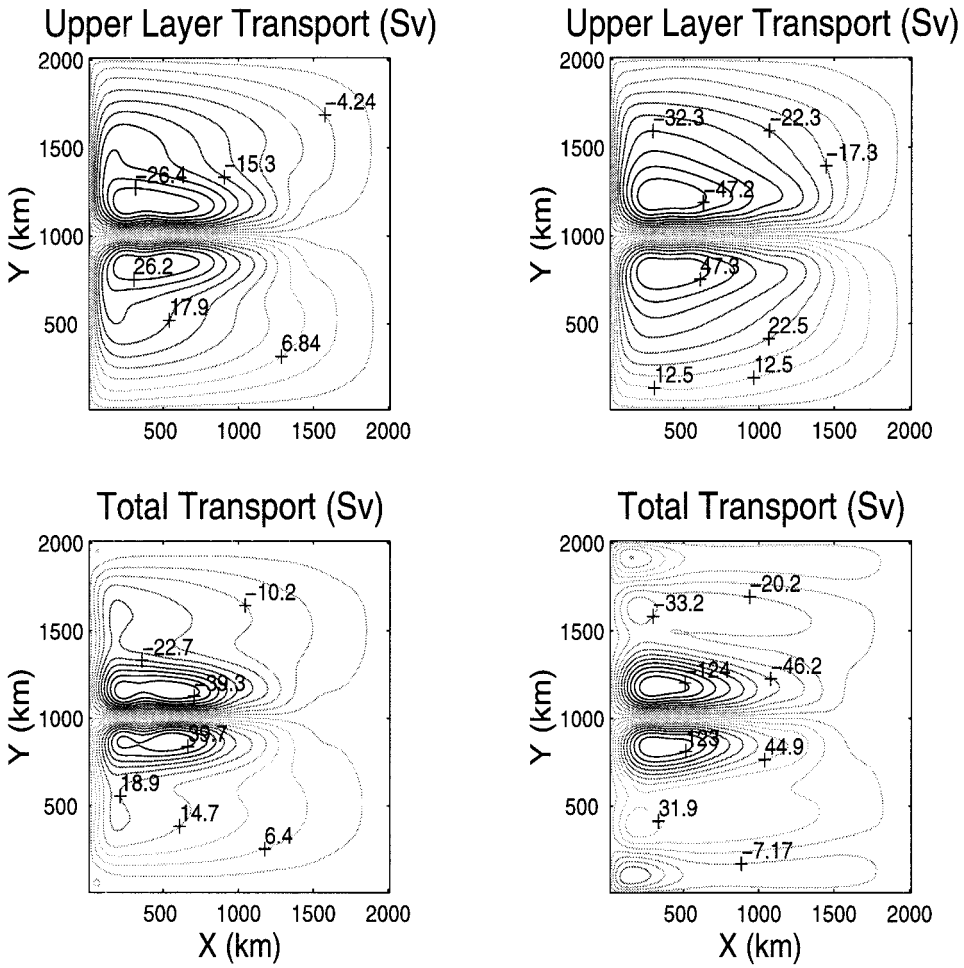

FIG. 4. Upper layer and total transports. These means were extracted from a 200-yr experiment with feedback and stochastic forcing. The average structures are essentially symmetric about the central latitude, and the central, western region of the model is dominated by inertial recirculations. The left-hand column used $\mu_o = 2.5 \times 10^{-6}$ m s^{-1} and the right-hand column $\mu_o = 5 \times 10^{-6}$ m s^{-1}; other parameters were identical.

entiated by the presence or absence of noisy forcing. In the latter case, ocean variability is due entirely to intrinsic variability. The temperature spectra for these two uncoupled runs are statistically indistinguishable and, in fact, almost identical. Given this overlap, the two uncoupled curves were not individually labeled.

Other significant features of these curves are that the uncoupled models are essentially red through much of the decadal to centennial band (with a white behavior beyond ~50 yr). Both uncoupled curves obey a -3 law, as does the coupled curve until about 10 yr. Beyond this, the coupled curve tends to white behavior.

Figure 5 shows that the primary effect of coupling is to generate white interdecadal ocean SST variability. This differs significantly from linear wave models where the roll off to a white spectrum from a red spectrum is present in uncoupled results. In the linear models, the presence of comparable spectral peaks in both oceanic and atmospheric data was taken as the indication of coupled dynamics. In our nonlinear model, it is the presence of a largely white low-frequency oceanic spectrum, on top of which spectral extrema are found, that indicates coupling.

c. What determines SST?

Figure 6 compares the SST spectra from the nonlinear model with that computed from the linear waves model. The two smooth curves represent $f = 0.2\ \mu_o\,\mathrm{K}^{-1}$ (with feedback) and $f = 0$ (without feedback). Note that the uncoupled, $f = 0$ case has an associated spectra that is essentially red, with a roll-off point at a few years. The coupled case, labeled $f = 0.2$, shows a spectral peak around 3 yr, and suppression for lower frequencies. The remaining curve is the temperature spectrum from the standard coupled model. This spectrum is characterized by elevated variance at low frequencies (by a factor of roughly 30) relative to the linear coupled curve and is

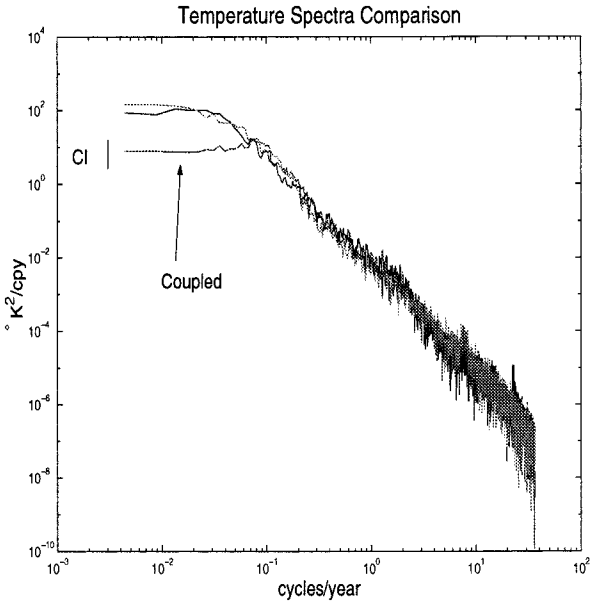

FIG. 5. Temperature spectrum from the standard coupled experiment, compared to spectra from the standard uncoupled runs with and without noise. The nonlinear, coupled model is damped at the low-frequency end relative to the uncoupled models, indicating an oceanic suppression of temperature variance by coupling. The vertical bar indicates the 95% confidence interval.

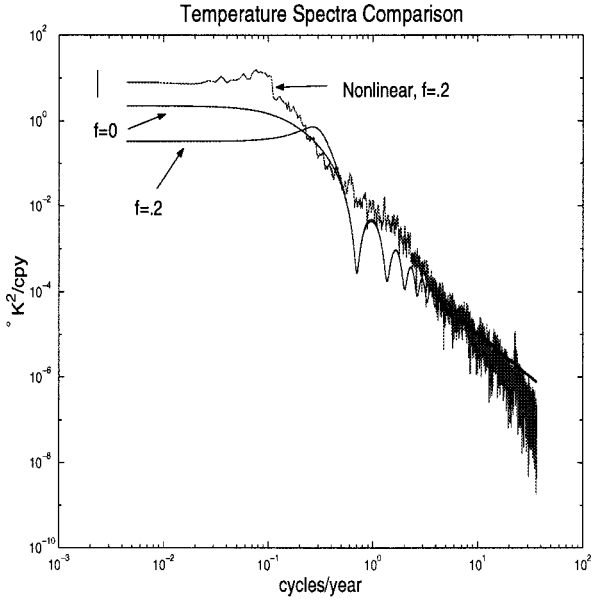

FIG. 6. Comparison of temperature spectra. The analytical solutions for SST subject to linear baroclinic waves for the cases $f = 0.2\ \mu_o$ K^{-1} and $f = 0\ \mu_o K^{-1}$ appear as the smooth lines. These are compared to the temperature spectrum from the present model, which computes the intergyre heat exchange from the nonlinear QG model. The vertical bars show 95% confidence intervals.

broadband. This comparison, which is typical of the several experiments we have conducted, demonstrates the linear wave model is a poor quantitative predictor of the ocean temperature spectrum.

If it is not linear waves, what determines SST? Manipulating (10) demonstrates

$$E_T = \frac{E_{\mathrm{HF}}}{4\pi\omega^2 + \lambda^2} + \frac{\hat{\alpha}^2 E_n}{(4\pi\omega^2 + \lambda^2)} + \mathrm{CC}, \quad (13)$$

where E_{HF} denotes the intergyre heat flux spectrum, E_n the atmospheric noise spectrum, and CC the cross spectrum of intergyre heat flux and atmospheric noise. The left-hand side of (13) is compared with the first two terms on the right-hand side in Fig. 7, where data from the standard coupled experiment has been used. The two top lines, which are essentially indistinguishable in the low-frequency band, represent the temperature spectrum and the cross-gyre heat transport spectral contribution. The remaining line is the input due to the NAO noise forcing. The change in character from high to low frequencies is clear, with temperature jointly influenced at short timescales by the atmospheric and oceanic heat fluxes, and dominated at longer timescales by oceanic intergyre heat flux. [The last term in (13) is similar in amplitude to the noise spectrum, and is not shown here.] The transition point occurs at approximately the annual period. This plot emphasizes that in the critical range of ocean SST damping, intergyre advection controls SST.

d. A simple conceptual model

Although our model is nonlinear, and therefore unlikely to be completely analytically tractable, we have hit upon a conceptual model that aids in understanding

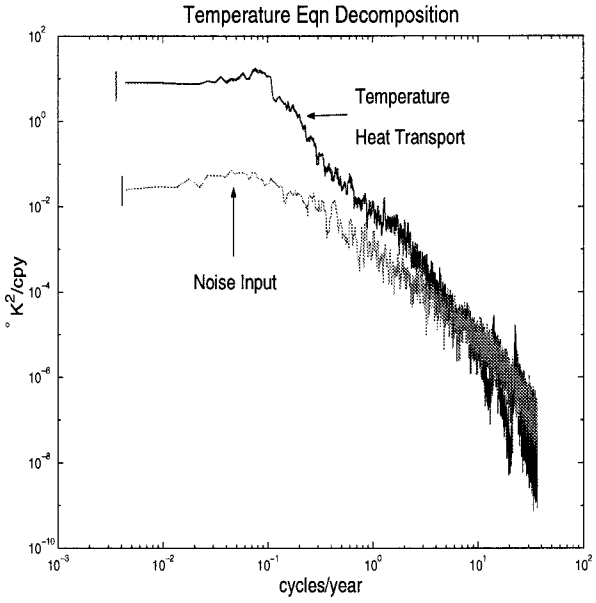

FIG. 7. Spectral temperature equation decomposition. The various inputs to SST are displayed. At high frequencies, noise and heat flux jointly determine the temperature frequency response. Ocean heat flux dominates at lower frequencies. The vertical bars show 95% confidence intervals.

the above results and also appears to be essentially a concise analytical statement of this nonlinear problem.

Ocean-only dynamics control SST variability by intergyre heat flux as essentially a red process. This is seen in Fig. 5, where SST spectra show a -3 slope through the interdecadal band for both uncoupled experiments. This may be partially understood as lower-frequency variability being more efficient at intergyre heat flux than high-frequency variability. We model intergyre heat flux (HF) therefore as

$$\widehat{\mathrm{HF}} = \frac{\Gamma \mu_o \hat{s}}{\omega^\nu} + \widehat{\mathrm{HF}}' = \frac{\Gamma \mu_o \hat{s}}{\omega^\nu} + \frac{\gamma \hat{w}_e' \hat{\phi}(\omega)}{\omega^\nu} \quad (14)$$

where ''hats'' imply Fourier transforms, red processes are represented by a $\omega^{-\nu}$ law, Γ scales the first input into the units of K m (s cpy)$^{-1}$, and γ does the same for the second input. The first input represents the effect of intrinsic oceanic variability on oceanic heat flux, and therefore is written as dependent on the mean Ekman pumping μ_o. The coefficient $\hat{s}$ is a stochastic variable with unit variance and appears because in any experimental realization of oceanic heat flux, the spectral amplitude at a given frequency will be random. The second flux input is due to the time-dependent Ekman pumping and is therefore written using $\hat{w}_e'$, the Fourier transform of the random variable $a(t)$. The quantity $\hat{\phi}(\omega)$ represents a phase function with unit amplitude. Its purpose is to distribute the spectral amplitude for the atmospherically forced intergyre heat flux between real and imaginary parts. This flux is also written as red to imply it is more efficient at lower frequencies than higher. To the extent second input involves an adjustment process, as will be argued shortly, at frequencies beyond the adjustment timescale, the system should be close to equilibrated and behave similarly to the mean forcing effect. There is also empirical evidence supporting our power-law choice. The uncoupled SST spectra in Fig. 5, are indistinguishable, hence the model intergyre heat flux characteristics are insensitive to the presence of stochastic Ekman pumping. This is consistent with choosing the power law of the second input in (14) to be the same as the first.

If we now invoke the coupling law (4), the conceptual SST spectrum is

$$E_T = \frac{\Gamma^2 \mu_o^2 + \gamma^2 \kappa^2 E_n + 2\hat{\alpha}\gamma\kappa E_n \omega^\nu \hat{\phi}_r + \hat{\alpha}^2 E_n \omega^{2\nu}}{\omega^{2\nu}\left[4\pi^2\omega^2 + \lambda^2 + \left(\frac{f\gamma}{\omega^\nu}\right)^2 + \left(\frac{4\pi\omega f \gamma \hat{\phi}_i}{\omega^\nu} - \frac{2 f \gamma \lambda \hat{\phi}_r}{\omega^\nu}\right)\right]}, \quad (15)$$

where it has been assumed the random variate $\hat{s}$ is uncorrelated with $\hat{N}$ and the quantities $\hat{\phi}_{[i,r]}$ denote the real and imaginary parts of $\hat{\phi}$. This spectrum is red for high frequencies and rolls off to a white spectrum

$$E_T = \frac{\Gamma^2 \mu_o^2 + \gamma^2 \kappa^2 E_n}{\gamma^2 f^2} \quad (16)$$

for frequencies low as compared with

$$\omega_c = \left(\frac{f\gamma}{\lambda}\right)^{1/\nu}. \quad (17)$$

Spectral shapes like those in Fig. 8 emerge, given flexibility in choosing γ, $\hat{\phi}$, and Γ. A simple fit to the low-frequency limit of the standard coupled experiment and to a roll-off point at 10 yr results in the spectrum appearing on the left in Fig. 8. The power-law ν was chosen from the model spectra, the Γ and γ values obtained from the fit appear in the plot and, for illustrative purposes, the phase function was set to $\hat{\phi} = 1 + 0i$. (Constraints on $\hat{\phi}$ are discussed later, but these conceptual model spectral shapes are not sensitive to $\hat{\phi}$ variations.) To the extent the adjustable parameters reflect the turbulence of the mean state and adjustment processes, they are poorly understood and worth investigation from first principles. We show on the right the pumping spectrum predicted by the conceptual model, and compare it with data from the standard coupled experiment. The model pumping is further decomposed into its constituents, consisting of the feedback input and noise. This plot illustrates both the skill of the conceptual model and that in the interdecadal band, the pumping is completely controlled by SST.

Pressing this simple and ad hoc model further, we test its predictions that the roll-off frequency depends on f [see (17)], and that at lower frequencies, the spectral suppression should be greater for greater coupling [see (16)]. Two indirect pieces of evidence, already discussed above, consistent with this are the dependence of the roll-off on nonzero coupling. This appears in the plots of uncoupled SST in Fig. 5. The red spectra of both uncoupled experiments through the interdecadal band is consistent with the uncoupled limit of (15). A more direct test has been performed using the standard parameter settings subject to the modification that $f = 0.5\ \mu_o\ \mathrm{K}^{-1}$. It is unlikely that the coupling feedback on the atmosphere of oceanic SST is as big as this. This calculation is meant only as a test.

The SST spectra from this experiment and from the standard coupled experiment appear in Fig. 9, where a linear, rather than log, format has been chosen. The differences in these spectra are not large, and certainly

not significant at the 95% confidence level, but throughout the frequency band of interest, both predictions hold true.

Given the crudeness of the conceptual model, its ability to capture the essential SST spectral behavior of the coupled model, including the SST spectral extreme, is encouraging. We therefore ask what the model represents physically that is responsible for those behaviors. The roll-off to a white spectrum clearly requires coupling. The mechanics responsible for the suppression can be investigated by analyzing the cross spectrum of the two oceanic heat flux inputs. Straightforward algebra yields

$$\langle \gamma \hat{w}_e'^* \hat{\phi}^* \mu_o \Gamma \hat{s} \rangle = \frac{\left(\lambda - \dfrac{f\gamma\hat{\phi}}{\omega^\nu} - 2\pi i\omega\right)\dfrac{f\Gamma^2\mu_o^2\gamma\hat{\phi}^*}{\omega^\nu}}{\left(\dfrac{f\gamma}{\omega^\nu}\right)^2 + \lambda^2 + 4\pi^2\omega^2 + \left(\dfrac{4\pi\omega f\gamma\hat{\phi}_i - 2f\gamma\lambda\hat{\phi}_r}{\omega^\nu}\right)}, \tag{18}$$

where the angle brackets ($\langle\ \rangle$) denote an ensemble average and the (*) a complex conjugate. The low-frequency limit of (18) shows

$$\lim_{\omega\to 0} \langle \gamma \hat{w}_e'^* \hat{\phi}^* \mu_o \Gamma \hat{s} \rangle = -\mu_o^2 \Gamma^2, \tag{19}$$

implying that at low frequency the two oceanic heat flux inputs are in opposition.

It is also instructive to evaluate the low-frequency limit of the intergyre heat flux spectrum from the conceptual model

$$E_{\rm HF} = \left\langle \left(\frac{\Gamma\mu_o\hat{s} + \gamma\hat{w}_e'}{\omega^\nu}\right)\left(\frac{\Gamma\mu_o\hat{s} + \gamma\hat{w}_e'}{\omega^\nu}\right)^* \right\rangle = \frac{\Gamma^2\lambda^2\mu_o^2}{f^2\gamma^2}, \tag{20}$$

where atmospheric noise has been neglected, and it is seen that the leading two contributions, proportional to $\omega^{-2\nu}$ and $\omega^{-\nu}$, from the two inputs cancel each other.

To make sense of these results, it is convenient to rewrite the Fourier transformed heat equation as

$$-2\pi i\omega\hat{T}_s\left(\underline{\frac{\gamma f\hat{\phi}}{\omega^\nu}} - \lambda\right)\hat{T}_s = -\underline{\frac{\Gamma\mu_o\hat{s}}{\omega^\nu}} + \frac{\gamma\kappa\hat{\aleph}}{\omega^\nu} + \hat{\alpha}\hat{\aleph}, \tag{21}$$

where $\hat{\aleph}$ is the Fourier transform of the atmospheric noise N and the two flux contributions have been explicitly written. The physical space SST equation abstracted from (21) can be written

$$T_{st} + \underline{\mathrm{HF}_f(\overline{T}, t)} = \underline{\mu_o\Gamma m(t)} - \lambda T_s + \hat{\alpha}N, \tag{22}$$

where $\overline{T}$ represents a filtered SST, that is, an average of SST over past values. (The lagging of the feedback flux behind SST is insured in the conceptual model if the proper sign is chosen for $\hat{\phi}_i$.) The quantity HF_f denotes the feedback-driven heat flux and its dependence on $\overline{T}$ and t implies that it represents a time-dependent process whose amplitude is sensitive to $\overline{T}$. The above is a stochastically forced equation with noise sources on the right, the first of which is the intrinsic variability flux driven by the ocean. The cancellation in the net oceanic heat flux inherit in (20) implies the leading-order low-frequency balance in (21) is between the two underlined terms. (Note this balance accounts for the low-frequency limit of the conceptual SST spectrum.) The equivalent balance in (22) is also between the underlined terms. Thus, feedback gives the system a way to balance the intrinsic oceanic heat flux at leading order. Corrections to this leading-order temperature are governed by the more classic mechanics of time dependence and relaxation.

Essential similarities between the behavior of this nonlinear model and the linear wave models are also underscored by (21) and (22). Given their relatively weak role in determining SST, the two stochastic atmospheric inputs in (21) can be neglected. Their role as forcing agents is filled by the oceanic intrinsic heat flux that may thus be viewed as analogous in effect to the stochastic atmospheric heat flux of the linear models. At low frequencies, the ocean feedback response opposes this heat flux, again in analogy to the linear models in which the linear ocean heat transport opposes the sense of the atmospheric heat forcing.

Analysis of the QG model output shows that net oceanic heat flux is balanced by relaxation, that is, $\mathrm{HF} = -\lambda T_s$ [see also (20)], implying net oceanic heat flux is directed up the anomalous temperature gradient. Equivalently, HF is southward for high T_s and northward for low T_s. The clear indication from Fig. 5 is that coupling introduces a negative feedback on SST. Coupling, of course, implies the presence of the feedback flux that, to be damping, must be directed downgradient. [This is insured in the conceptual model if $\hat{\phi}_r(\omega \to 0) < 0$.] Since the net flux is upgradient, the larger of the two inputs to net oceanic heat flux must be the intrinsic variability. The residual, or net, heat flux is that left over from the opposition of the two inputs.

An SST cycle at low frequencies therefore follows the intrinsically driven oceanic flux. Such flux will wane in strength from an extreme due to intrinsic causes,

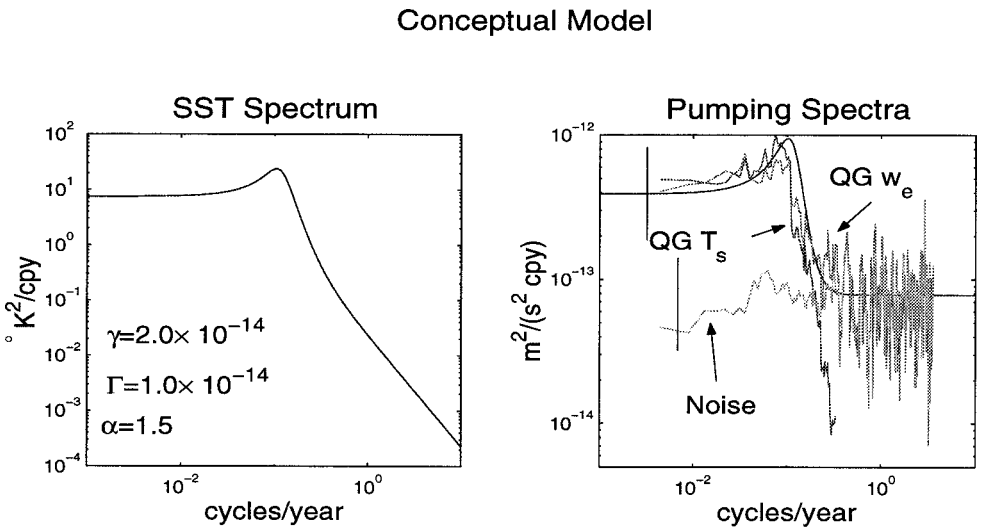

FIG. 8. Example of conceptual spectra. The parameters Γ and γ have been chosen by fitting the low-frequency limit of model SST spectra and setting the roll-off point to 10 yr. The temperature spectrum appears on the left. On the right, the conceptual pumping spectrum is compared to standard coupled model data. The model pumping constituents, i.e., feedback and noise, are also shown. The vertical bars in the pumping spectra show 95% confidence intervals.

leading the net flux to eventually turn downgradient. The strength of the SST anomaly will fade and with this will come a decreasing strength of the feedback flux. Eventually, the net flux will drive a reversal in SST and an opposite-signed SST anomaly will grow. An opposite-signed feedback flux will follow with an appropriate temporal lag, and arrest the strength of the net ocean flux, thereby restoring balance in the white part of the SST spectrum.

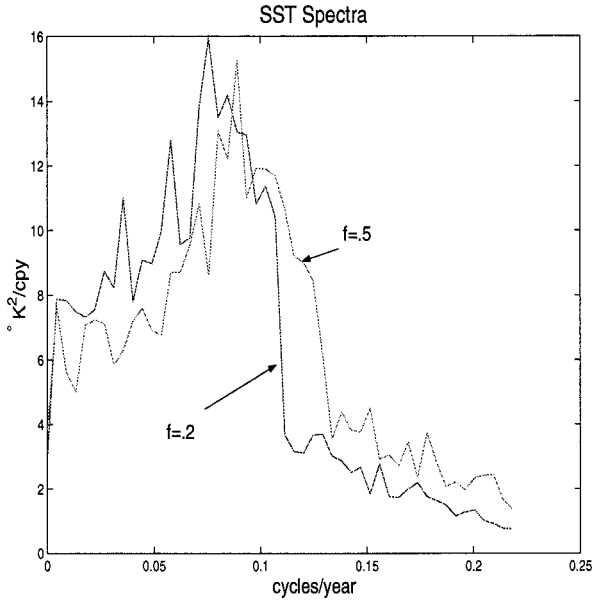

FIG. 9. SST spectra from the standard coupled run and one with $f = 0.5\ \mu_o\ \mathrm{K}^{-1}$. Other parameters were standard. This is a linear, rather than log, plot to draw out the relative structure.

The explanation for the peak, always occurring near the critical frequency, is also found in (21) and (22). At higher frequencies, the adjustment process driving the feedback flux having not completed, will yield upgradient values for both the feedback and intrinsic heat fluxes (this occurs in the conceptual model if $\phi_r > 0$). The heat equation near this frequency can thus naturally generate enhanced variance.

The spectral enhancement at high frequency associated with strong coupling (Fig. 9) may be interpreted as the system using the inphase oceanic heat fluxes more effectively at frequencies higher than ω_c to increase SST variance. At low frequencies, the cooler set point of the system reflects more efficient use of anomalous temperature to cancel the intrinsically driven heat flux.

e. What is the spatial pattern of the feedback flux?

The results of an EOF analysis of the standard coupled run appear in Fig. 10. Monthly upper-layer pressure fields were averaged using a simple 12-month boxcar filter and EOFs were extracted from the averaged datasets. The variance accounted for by these modes are 38%, 13%, and 11%, respectively. The second mode is reminiscent of one of the leading modes computed by Berloff and McWilliams (1999) in their two-layer study of nonlinear gyre variability. Clearly, all of these modes are associated with inertial recirculation variability, rather than with basin-scale baroclinic wave modes. In fact, the next several EOFs are also associated with the inertial recirculation. We are unable to find evidence of basin-scale wave modes in the first 10 EOFs.

The first and third annual average data EOFs are the modes governing the oceanic heat flux variability in this

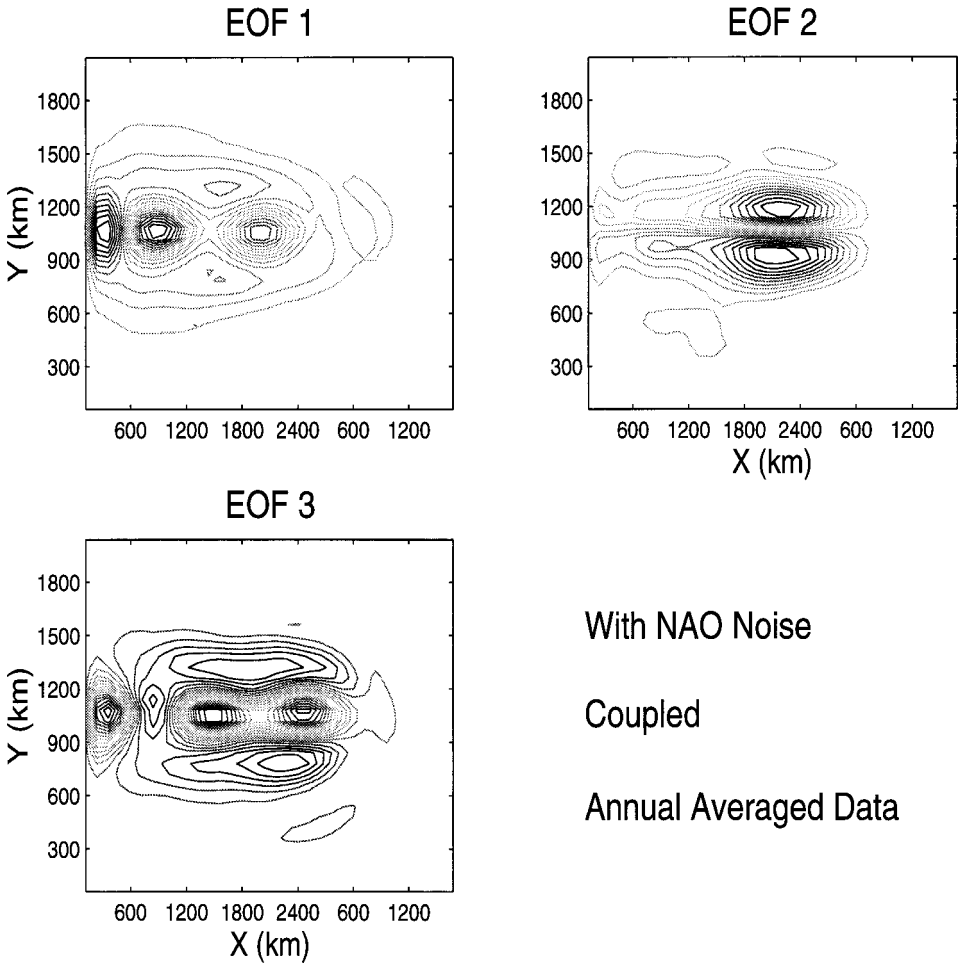

FIG. 10. The three leading EOFs from the nonlinear coupled run. Model data averaged over a year were used. The variances of these modes were 38%, 13%, and 11%, respectively. The first and third modes show standing eddy patterns.

model. This appears in the coherences between the heat flux time series and the principal components for the first three modes (Fig. 11). Also shown in this plot is the coherence between two random number series of the same length of the principal components, analyzed identically to the data. Note that the first and third EOFs are significantly coherent with SST across the interdecadal band.

WHAT ARE THE LEADING EOFS IN THE COUPLED RUN?

We now interpret physically the leading annual-averaged EOF from the coupled run. Figure 12 shows a composite streamfunction made from the mean streamfunction field and the leading annual-averaged EOF. The maximum to minimum range of the principal component was roughly 1.5 to -1.5 and this value was used to scale the EOF. The upper-left-hand panel is a point of maximum principal component and the upper-right panel a point of vanishing principal component. The lower-left panel is a point of minimum principal component. The sequence is meant to convey the circulation variability associated with the leading averaged EOF. For comparison, in the lower-right-hand panel, we show the results of a steadily forced experiment. This is a plot of a 20-yr average, in which the Ekman pumping was held fixed with a composite field made from the mean and the variable Ekman pumping fields in (2) and (3), respectively, such that the anomalous Ekman pumping forced a downwelling at the mean intergyre boundary. The shape of this field appears in the lower panels of Fig. 2. Note that the streamfunctions in the lower panels of Fig. 12 are similar. The mirror image of the lower-right panel resembles the upper-left-hand panel.

This plot argues that the leading annually averaged EOF is measuring the drive of the circulation toward the equilibrium state associated with the perturbed Ekman pumping. The variability associated with it may therefore be interpreted as a directly forced response of the gyre. The smaller amplitude of the perturbation in the composite plots reflects partly that the perturbation

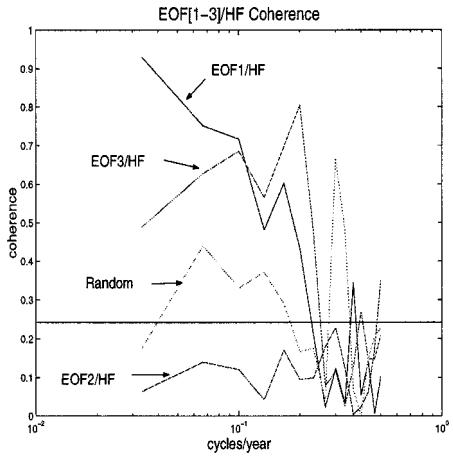

FIG. 11. Coherence between the first three EOFs and the oceanic heat flux. The average coherence computed from two random number sequences analyzed identically to the principal components is roughly 0.24 and indicated by a solid line. Also shown is coherence as a function of frequency for these two random series in the curve labeled ''random.'' Note the significant coherence in the interdecadal band between the first and third EOFs and the oceanic heat flux. The second EOF shows no significant coherence across the frequency bands.

forcing is stochastic, rather than fixed. The small scales in the first and third EOF reflect the mesoscale undulations of the separated jet (see Cessi et al. 1990). The nature of the oceanic heat fluxes associated with the leading EOF is shown in Fig. 13, where the heat flux computed at the central latitude of the EOFs is plotted. Note, the farthest west, cyclonic anomaly pressure anomaly of the first EOF does not control the oceanic heat flux, even though it has the largest amplitude of the mesoscale features. The next meander, which is much broader, contributes much more effectively here to generate the net transport (in this case a northward transport). This plot suggests an important oceanic heat flux role for the standing eddies in the ocean circulation.

In a sense, the importance of the NAO spatial pumping structure to the ocean variability argues that the temporal oceanic response is governed by the NAO, as opposed to the response of an ocean model without knowledge of NAO fields. In the latter case, spatial patterns associated with intrinsic variability would dominate. While we agree with the importance of the NAO, its role requires qualification as suggested by the conceptual model, and as is discussed in the next sections.

f. The source of the temporal ocean variability

Having determined that spatial variability centered in the inertial recirculation controls the anomalous SST gradient, it is natural to explore the source of the temporal ocean variability. We test the conceptual model idea that ocean intrinsic variability energizes the ocean coupled temporal variability. Given the dominance of SST in the Ekman pumping spectrum, this implies the atmospheric variability in the interdecadal band is under the control of the ocean variability.

To address this issue, we examine an experiment with no stochastic pumping, that is, one using the standard coupled parameters modified by $\kappa = 0$. The ocean is aware of the atmosphere, however, through the presence of the NAO anomalous spatial Ekman pumping pattern and atmospheric stochastic heat fluxes.

Comparisons of various spectral measures of this experiment and the standard coupled experiment are given in Fig. 14. The upper row compares the SST and pumping spectra from these two experiments. The important point is that the low-frequency SST suppression is present in both. The noticeable difference is that the suppression is stronger in the standard experiment, a result that probably reflects greater excitation of the NAO wind pattern in the latter. The lower row shows the coherence and phase data as computed from the oceanic heat flux and temperature time series from the coupled experiment without noise. These plots possess the same model variable characteristics in the interdecadal band as those from the standard coupled run. They do differ in the superannual band, with the experiment without noise showing no coherent signal between oceanic heat flux and SST. This is a frequency band where the efficiency of the intergyre heat transport is not yet great, and the model is dominated by the atmospheric stochastic heat flux.

As the coupled experiment with $\kappa = 0$ has no stochastic momentum forcing at all, we conclude that the dominant SST behavior in this model reflects oceanic intrinsic variability and that atmospheric stochastic momentum input is of secondary importance. The minimal, broader, interpretation of this result is that oceanic intrinsic variability should not be neglected as a source for SST variance in the coupled climate system.

These points are consistent with the right-hand panel of Fig. 8, which shows the spectral decomposition of the Ekman pumping variability from the standard coupled experiment. The inputs to the Ekman pumping are noise and the temperature feedback and it is clear in the interesting interdecadal band that the atmosphere is dominated by SST. At higher frequencies, the noise dominates, with the important comparison that the low-frequency energies are greater by a significant amount. Recalling some earlier results, the intergyre heat flux dominates SST in our experiments, and intergyre flux depends on Ekman pumping variability. This, however, is controlled by SST, and that variability is modestly sensitive to atmospheric noise. Thus, we find ourselves in the interesting position that the atmospheric variability is under the control of oceanic processes. In this regard, the nonlinear model differs significantly from linear waves models, where oceanic variability is driven solely by atmospheric processes.

Temperature variance may also be viewed as a self-limiting process, an interpretation suggested by the pumping spectrum. The similarity between the two SST

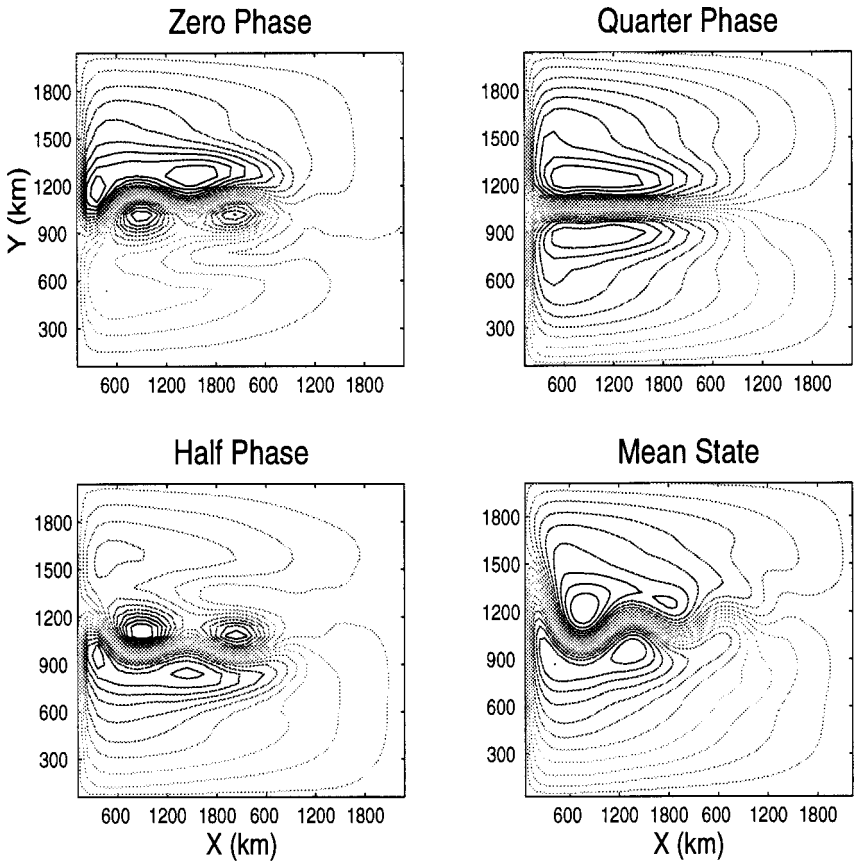

FIG. 12. Variable upper-layer streamfunctions as constructed by adding the mean streamfunction and the leading annual-averaged EOF. The point of maximum principal component amplitude appears in the upper left, at quarter phase in the upper right, and at half phase in the lower left. For comparison, in the lower right we show the mean state streamfunction obtained from an experiment with steady, but asymmetric wind stress forcing patterned on the NAO forcing.

spectra for the standard uncoupled cases can be taken to mean the level of the Ekman pumping variability is too weak to dominate intergyre flux over intrinsic variability. Coupling pumping to the strongly red SST spectrum however, forces pumping variance to higher levels, where the forced intergyre flux can significantly contribute. This, of course, damps SST variance.

g. How important is the NAO spatial structure?

If the stochastic temporal NAO input is secondary in importance, one asks if the NAO spatial input is critical. Here we discuss an experiment which, at least partially, addresses this point. We question how sensitive the results are to the detailed structure of the anomalous pumping field. The answer is that the spatial NAO anomaly field is of first-order importance to the standard coupled model behavior.

The experiment described here used the standard coupled parameter set. The difference from the standard coupled run was that the anomalous temporal Ekman pumping fed into variability of the mean Ekman pumping spatial structure, rather than the NAO Ekman pumping structure

$$w_e = [\mu_o \pm a(t)] \sin(\pi y/L) \tag{23}$$

and the NAO pumping structure was absent. The data were analyzed similarly to earlier results, and interpreted from the perspective that if the results were similar to the standard coupled run, the leading-order behavior could be argued to be insensitive to the particular form of the NAO pumping. The outcome, however, was unambiguously inconsistent with this view. Figure 15 compares SST spectra from the standard coupled run with those from the standard uncoupled runs and from the latest, nonstandard, coupled runs. Two curves from the latter category are shown, differentiated by the sign assigned to the Ekman pumping perturbation [i.e., one of the two signs in (23) was chosen]. These phases are labeled in the plot. The point is that spectral suppression in the interdecadal band is absent in all but the standard coupled experiment, and therefore is clearly a property dependent to some degree on the shape of the anomalous pumping field.

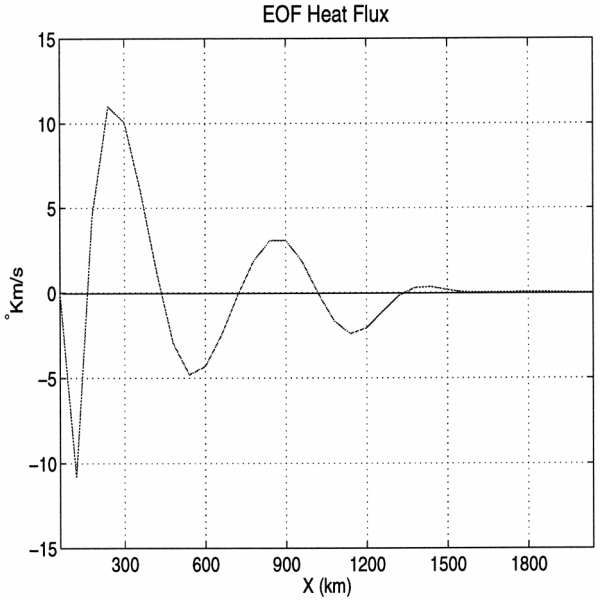

FIG. 13. Leading EOF intergyre heat flux pattern. This was computed from the structure of the leading annually averaged EOF pattern at the intergyre latitude. Note the standing eddy pattern is the dominant input to the heat flux.

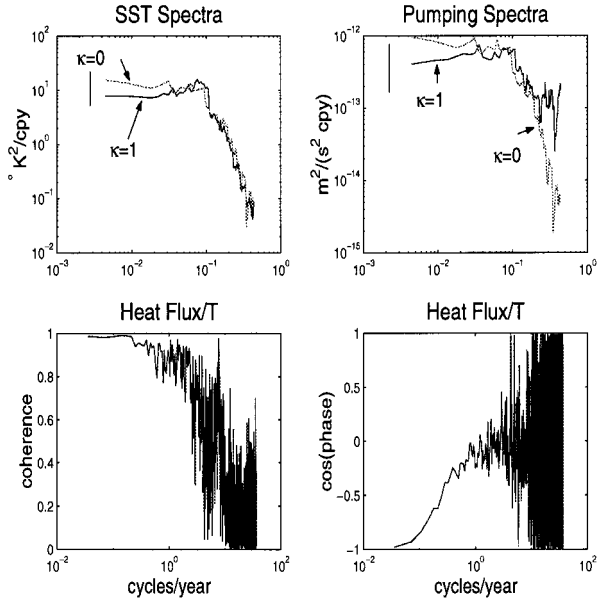

FIG. 14. Spectral measures from an experiment with coupling but no atmospheric noise. The top left compares SST and the top right pumping, with the spectra from the standard coupled run. The bottom left is coherence between intergyre heat flux and *T* and the bottom right cos of the phase between heat flux and *T*. The latter two are both from the coupled experiment without noise. The bar in the upper panels is the 95% confidence interval.

4. Discussion

The role of the ocean in midlatitude coupled climate variability has been examined using a nonlinear, quasigeostrophic ocean forced by a simple, but responsive atmospheric model. The study here is patterned after process coupled climate models that have been offered for their relevance to the observed variability of the North Atlantic Ocean. Our thesis is that it is the inertial recirculations of the gyres that dominate oceanic variability, rather than waves. The experiments discussed here support this view.

We find that the predictions for SST spectra based on the linear waves model are inaccurate when compared to the spectra computed from the nonlinear model. Instead, we propose a simple model, based dynamically on ocean intrinsic variability, that explains the results of our numerical experiments. The main feature of the numerical experiments is that SST is suppressed at low frequencies due to coupling. A secondary feature is that SST spectra develop extrema in the near-decadal band. Both of these features are found in our conceptual model and explained by competition between the background mean state–driven intergyre heat flux and a feedback-driven intergyre flux. Both the SST and atmospheric spectra are dominated by the ocean input. The most significant atmospheric role in this model is in selecting the spatial structure of the atmospheric response to the anomalous ocean–atmosphere heat exchanges. There is a dependence of the SST spectra on this structure, so this is not minor. Evidence also suggests the NAO noise forcing helps to organize the oceanic response, probably

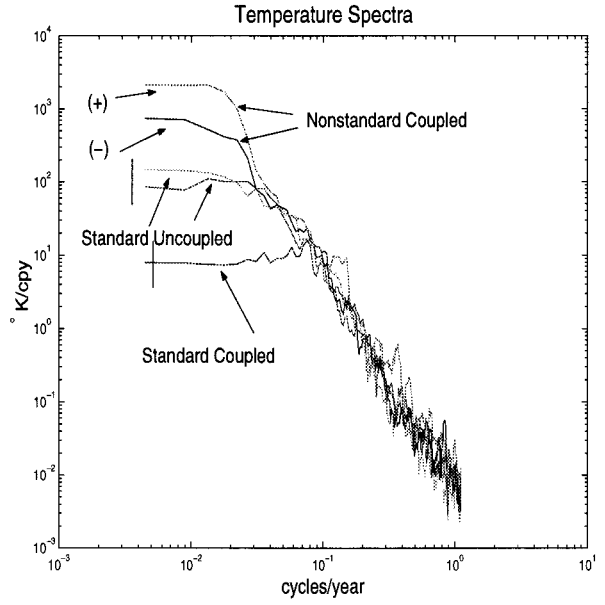

FIG. 15. SST spectra comparisons from the standard coupled experiment, the standard uncoupled experiments, and the nonstandard coupled experiments. The nature of the SST response clearly depends upon the structure of the anomalous pumping field. The 95% confidence interval is denoted by the bar.

through an added excitation of the atmospheric NAO structure.

a. Comparisons with observations

Interest in these models has been motivated recently by analyses of North Atlantic long-term observations. In particular, Czaja and Marshall (2000) computed SST spectra for subdomains of the North Atlantic located in the subpolar and subtropical gyres. The test areas were both located in the western domain of the basin and on either side, approximately, of the climatological Gulf Stream track. Those spectra showed peaks for both boxes at frequencies slightly lower than decadal. There was some asymmetry between the two, with the northern box showing a broader peak and somewhat higher variance in the near-centennial band. The spectral peak of the temperature difference time series stood out from the background by roughly a factor of 3–5. The lower-frequency spectral structure is difficult to gauge, given a lack of data, but is not inconsistent with an essentially white behavior. In the interannual band, there is a tendency for variances to be lower, with something like a factor of 10 standing between the variance at 5 yr and the spectral peak. Again there is some asymmetry between the two boxes.

Atmospheric variables also show structure in these same bands. The analysis in Czaja and Marshall (2000) is limited to sea level pressure (SLP), but it is seen that a peak exists in the so-called Greenland–Iceland record. This behavior differs from that of the Azores record, where variance levels show no clear peak. The overall NAO record is made of the difference of these two time series, so the NAO spectrum is dominated by the Azores record at low frequencies. The peak in the Greenland–Iceland record has suggested that this part of the North Atlantic may well be experiencing local dynamics distinct from those in operation near the Azores. The SLP peak is roughly a factor of 3–6 larger than the background and, while the lower- and higher-frequency structures of the spectra are difficult to gauge, they are not inconsistent with white on both sides.

We do not have SLP in our model; pumping is used as a proxy for all atmospheric variables. Nonetheless, the above spectral descriptions are clearly reminiscent of those resident in the present model. This is true for the frequency bands involved as well as for the observed levels of peak amplification. Of course, similar comparisons are also found using the linear waves model, but it is fair to suggest the nonlinear model explains these observations equally well. We therefore offer the nonlinear model as a competitor to the linear waves model.

b. Contrasts with linear dynamics

Despite their spectral similarities, there are several climatic implications of these models that are really quite distinct. Most importantly, the present nonlinear system is not fundamentally dependent upon the atmosphere for its variability. Rather, it is the oceanic intrinsic variability that energizes the entire process. Another distinction is found in the nature of the atmospheric variability. The linear waves model argue oceanic variability is dependent upon atmospheric driving and at best modifies the atmospheric spectra. In the present nonlinear problem, the Ekman pumping, itself a proxy for the wind stress, is under the complete control of the SST in the interdecadal band. The SST in turn is dominated by the oceanic intrinsic variability, so atmospheric variability is controlled by oceanic processes. Third, in the linear waves model, the only effect of the coupling was to depress variance at lower frequencies, thereby enhancing peaks at intermediate frequencies. Here, the evidence pointing to coupling is not primarily in the peaks, which are really rather minor spectral features, but in the much stronger roll-off to a white spectrum.

The linear waves models of Jin (1997), Neelin and Weng (1999), and MJG can be discussed in terms of a delayed oscillator, where the delay is set by wave processes. While we question the adequacy of linear waves for this problem, given the importance of the adjustment process to the variable wind forcing, there is support in this work for the delayed oscillator concept. The timescales appropriate to this system are not the baroclinic transit times, but rather the adjustment times, or adjustment interval, of the inertial recirculations. This is a process whose dependence on model parameters is not known, but almost certainly depends upon advection speeds as well as deformation radii.

A different model, in which intrinsic variability was also important, was that of Cessi (2000, manuscript submitted to *J. Climate*), as well as the subsequent exploration of related systems (Gallego and Cessi 2000; Primeau and Cessi 2001). There is a distinction between the present atmospheric model and the one employed by Cessi (2000, manuscript submitted to *J. Climate*) in that hers was more complete. The intrinsic variability in that model arose due to temperature advection, but was centered primarily within the gyres, rather than between the gyres as here. In our opinion, this distinction reflects a lack of mesoscale dynamics in the Cessi (2000, manuscript submitted to *J. Climate*) ocean model, rather than the differing atmospheric models. Nonetheless, an interesting point is that explicit SST appears in her model and not in the present one. Literally speaking, there is no opportunity for advected SST anomalies within the gyres to affect the atmosphere in this study. Further work with a more complete SST model in the present setting is advisable.

c. Model criticism

While the spectra generated by the present nonlinear ocean model bear some interesting structure relative to

observed ocean and atmospheric spectra, there are significant model behaviors that are at odds with some observations and conventional ideas about North Atlantic climatic variability. We comment now on those.

Perhaps most important, the level of SST variance predicted by the model (± 2.5 K) is well in excess of the observed level (± 1 K). This is implicit in the insensitivity of the model to the atmospheric stochastic heat flux seen in section 3c. The generally accepted NAO paradigm is that the atmosphere to ocean heat fluxes control the NAO SST anomaly at leading order, and that the oceanic role is to modulate the SST signal. This basic balance is implicit in MJG, and, before that, in Frankignoul et al. (1997). The leading balance in the SST equation of the linear class of models is

$$\mathrm{HF} = -\lambda T_s + \hat{\alpha} N, \tag{24}$$

where the latter two terms are the largest of the three. The oceanic heat flux in this case is downgradient and is a perturbation on the atmospherically forced and maintained SST anomaly. The above differs from the leading-order balance of the present model, which is

$$\mathrm{HF} = -\lambda T_s \tag{25}$$

with the oceanic heat flux driven by intrinsic variability mostly balancing that due to feedback (i.e., the right-hand side is weak). An advantage of (24) is that the predicted SST amplitude is comparable to the observations whereas the present model predicts too great of an SST variance. Another related issue is that the linear models predict the anomalous atmospheric fluxes associated with the NAO [represented by $\hat{\alpha}N$ in (24)] are in phase with positive T_s. This appears consistent with observational analyses. The nonlinear model, however, suggests no particular relationship exists between anomalous atmospheric heat fluxes and the NAO.

Last, the model here employs a small basin (2000 km $\times$ 2000 km) relative to the North Atlantic (more properly sized at 6000 km $\times$ 6000 km). This decision was made for computational expedience, given the desire to explicitly resolve mesoscale dynamics and compute for hundreds of years and for several parameter settings. On the other hand, linear wave dynamics probably suffers as a result, for the reason that the inertial recirculations are unlikely to grow in size if the basin is increased, and thus wave propagation can proceed over the eastern parts of the basin as postulated in linear models. Along these lines, a recent study of Kravtsov and Robertson (2001, manuscript submitted to *J. Phys. Oceanogr.*, hereinafter KRG) suggests among other things a decreased sensitivity of SST to inertial recirculation dynamics in larger basins. Large-scale planetary wave propagation also appears in observations (Chelton and Schlax 1996; Hong et al. 2000). Miller and Schneider (2000) provide a recent review.

The above criticisms are serious and deserving of attention. The concern about basin size is currently under investigation, but we point out that the mass transports in this study have been tuned to match those observed in the North Atlantic. To the extent that the recirculations balance potential vorticity excesses in the general circulation, we might expect that appropriate levels of variability have therefore been captured here (but see below). In addition, the results of KRG may reflect a parameter setting that underestimates mesoscale variability.

Relative to the issues about the phasing of the NAO and anomalous heat fluxes, one wonders how well the relationship between anomalous atmospheric heat fluxes and SST have been defined for interdecadal frequencies. But, even aside from this, it is quite possible that some aspect of this model amplifies the intrinsic variability relative to the real ocean in an unrealistic way. The fact nonetheless remains that the mechanics described in this paper are apparently able to operate in a relevent frequency band and to produce by themselves spectral shapes that are like those observed. Indeed, one could damp the intrinsic variability in its effects on SST by a factor of 5 in the present model, and still expect them to be a dominating influence in determining SST. Last, although the net heat flux is upgradient, the sense of the oceanic feedback in this model is downgradient (i.e., the part of the oceanic heat flux proportional to the feedback parameter f is directed away from the SST anomaly maximum). This is in the same sense as the oceanic effect in the linear waves model, even if the mechanisms in operation are essentially different. The present model may thus be interpreted as emphasizing a different set of ocean dynamics capable of playing a comparable role to those forwarded in linear waves models.

One may also correctly question our ''atmospheric model,'' relating anomalous Ekman pumping to atmospheric noise and a direct SST feedback. Certainly many GCM studies argue against such a simple ocean–atmosphere coupling, particularly in midlatitudes. On the other hand, the recent analyses of Czaja and Marshall (2000, 2001) offer some observation support for the coupling expression.

These points emphasize the importance of determining the sensitivity of the present results to unexplored model variations. In our opinion, a particularly important issue along these lines is the impact of the spatial structure of the NAO pumping field, that is, what constitutes the critical aspect of the NAO pumping anomaly required to suppress SST. We do not have a definitive answer to this, but a reasonable speculation, consistent with our experiments, is that our NAO field breaks the symmetry of the mean pumping field. This is an aspect not found in either of the nonstandard coupled runs, where at all times subtropical gyre forcing was exactly the opposite of the subpolar forcing.

In view of this, it may be particularly relevant to break the symmetry of the mean forcing in future work. Berloff and McWilliams (1999) have recently argued for some dependence of both the structure of the leading

EOFs and their relative roles in explaining ocean variance on the degree of symmetry between the subpolar and subtropical gyre forcing. A second aspect of the mean state Ekman pumping field that neither this study nor that of Berloff and McWilliams considers is the well-known zonal tilt of the zero Ekman pumping line in the North Atlantic (Harrison 1988; MJG). The impact of this has been discussed in the context of the linear baroclinic wave models in MJG and its effects on the nonlinear problem would be interesting to explore. To the extent that the levels of intrinsic ocean variability depend on these features, their role may significantly influence the results.

It is also of paramount importance to supplant our atmospheric model, here given by (4), by a less restricted representation. At the same time, it is clear from this study that climate models overlooking intrinsic oceanic variability do so at their peril. Because the computational requirements of a coupled GCM working at eddy resolution, necessary for nonlinear dynamics to be realistically captured, are great, it is unlikely that a comprehensive study of the present type is possible using them. Intermediate complexity models with dynamics capable of resolving the eddies are required.

Acknowledgments. WKD is supported by NSF Grant ATM-9818628 and NASA Grants NAG5-7630 and NAG5-8291, the latter awarded in support of the NASA Seasonal to Interannual Prediction Project. The author wishes to acknowledge a number of interesting conversations with David Adamec, Arnaud Czaja, John Marshall, and Tony Sturges. Ms. J. Jimeian assisted with computational issues. This is a contribution of the Climate Institute, a Center of Excellence supported by the Research Foundation of The Florida State University.

REFERENCES

Berloff, P., and J. McWilliams, 1999: Large-scale low-frequency variability in wind-driven ocean gyres. *J. Phys. Oceanogr.,* **29,** 1925–1949.

Bjerknes, J., 1964: Atlantic air–sea interaction. *Advances in Geophysics,* Vol. 10, Academic Press, 1–82.

Bretherton, C., and D. Battisti, 2000: An interpretation of the results from atmospheric general circulation models forced by the time history of the observed sea surface temperature distribution. *Geophys. Res. Lett.,* **27,** 767–770.

Cessi, P., R. Condie, and W. Young, 1990: Dissipative dynamics of western boundary currents. *J. Mar. Res.,* **48,** 677–700.

Chelton, D., and M.G. Schlax, 1996: Global observations of oceanic Rossby waves. *Science,* **272,** 234–238.

Czaja, A., and J. Marshall, 2000: On the interpretation of the response of atmospheric models to prescribed time-varying *SST* anomalies. *Geophys. Res. Lett.,* **27,** 1927–1930.

——, and ——, 2001: Observations of atmosphere–ocean coupling in the North Atlantic. *Quart. J. Roy. Meteor. Soc.,* **127,** 1893–1916.

Frankignoul, C., and K. Hasselmann, 1977: Stochastic climate models. Part II: Application to sea-surface temperature variability and thermocline variability. *Tellus,* **29,** 289–305.

——, P. Müller, and E. Zorita, 1997: A simple model of the decadal response of the ocean to stochastic wind forcing. *J. Phys. Oceanogr.,* **27,** 1533–1546.

Gallego, B., and P. Cessi, 2000: Exchange of heat and momentum between the atmosphere and the ocean: A minimal model of decadal oscillations. *Climate Dyn.,* **16,** 479–489.

Haidvogel, D. B., J. C. McWilliams, and P. R. Gent, 1992: Boundary current separation in a quasigeostrophic, eddy-resolving ocean circulation model. *J. Phys. Oceanogr.,* **22,** 882–902.

Harrison, D., 1988: On the climatological monthly mean wind stress and wind stress curl fields over the world ocean. *J. Climate,* **1,** 57–70.

Holland, W., 1978: The role of mesoscale eddies in the general circulation of the ocean-numerical experiments using a wind-driven quasi-geostrophic model. *J. Phys. Oceanogr.,* **8,** 363–392.

Hong, B., W. Sturges, and A. Clarke, 2000: Sea level on the U.S. east coast: Decadal variability caused by open ocean wind-curl forcing. *J. Phys. Oceanogr.,* **30,** 2088–2098.

Hurrell, J., 1995: Decadal trends in the North Atlantic oscillation: Regional temperatures and precipitation. *Science,* **269,** 676–679.

Jin, F.-F., 1997: A theory of interdecadal climate variability of the North Pacific ocean–atmosphere system. *J. Climate,* **10,** 1821–1835.

Latif, M., and T. Barnett, 1994: Causes of decadal climate variability in the North Pacific/North Atlantic sector. *Science,* **266,** 634–637.

Marshall, J., H. Johnson, and J. Goodman, 2001: A study of the interaction of the North Atlantic oscillation with ocean circulation. *J. Climate,* **14,** 1399–1421.

Mathworks, 2000: Signal processing toolbox users guide, version 5. The Mathworks, Natick, MA, 872 pp.

Mehta, V., M. Suarez, J. Manganello, and T. Delworth, 2000: Oceanic influence on the North Atlantic oscillation and associated Northern Hemisphere climate variations. *Geophys. Res. Lett.,* **27,** 121–124.

Miller, A., and N. Schneider, 2000: Interdecadal climate regime dynamics in the North Pacific Ocean: Theories, observations and ecosystem impacts. *Progress in Oceanography,* Vol. 47, Pergamon, 355–379.

Münnich, M., M. Latif, S. Venzke, and E. Maier-Reimer, 1998: Decadal oscillations in a simple coupled model. *J. Climate,* **11,** 3309–3319.

Neelin, J., and W. Weng, 1999: Analytical prototypes for ocean–atmosphere interaction at midlatitudes. Part I: Coupled feedbacks as a sea surface temperature dependent stochastic process. *J. Climate,* **12,** 697–721.

Primeau, F., and P. Cessi, 2001: Coupling between wind-driven currents and midlatitude storm tracks. *J. Climate,* **14,** 1243–1261.

Rodwell, M., D. Rowell, and C. Folland, 1999: Oceanic forcing of the wintertime North Atlantic oscillation and European climate. *Nature,* **398,** 320–323.

Saravanan, R., 1998: Atmospheric low-frequency variability and its relationship to midlatitude SST variability: Studies using the NCAR climate system model. *J. Climate,* **11,** 1386–1404.

——, and J. McWilliams, 1997: Advective ocean–atmosphere interaction: An analytical stochastic model with implications for decadal variability. *J. Climate,* **11,** 165–188.